Unmanned Systems, Vol. 5, No. 3 (2017) 159–167

DOI: 10.1142/S2301385017400027

Unmanned Systems
http://www.worldscientific.com/worldscinet/us

Dynamic Characterization of Brushless DC Motors and Propellers for Flight Applications

Dominic Muzar, Eric Lanteigne*, Justin McLeod

Department of Mechanical Engineering, University of Ottawa, Ottawa, ON, Canada

Although there exist a number of accurate unmanned aerial vehicle (UAV) thruster models, these models require the precise measurements of several motor and propeller characteristics. This paper presents a simple motor and propeller model that relies solely upon data provided by manufacturers. The model is validated by comparing theoretical motor and propeller behavior to experimental results obtained from thrust tests in a wind tunnel. The objective is to provide an accurate yet simple model to facilitate the selection of appropriate brushless DC motor and propeller combinations for flight applications.

Keywords: Brushless DC motor; propeller; unmanned aerial vehicle.

1. Introduction

Electric motors offer a compact, power dense, and reliable power plant making them ideal for use in small unmanned aerial vehicles (UAVs). In particular, induction, brushed DC, and brushless DC motors are well suited to this application [1]. Among these, the brushless DC (BLDC) motor stands out on account of its high power density, efficiency, and reliability. The availability of small, inexpensive power electronics has made BLDC motors more cost-competitive and increasingly popular for UAV applications [1–6].

BLDC motors typically have permanent magnets integrated to the rotor while the stator houses the windings. They function similarly to synchronous motors, that is, by sequentially energizing the stator windings causing the rotor to turn due to alignment torque. The BLDC motor uses an Electronic Speed Control (ESC) circuit to perform the commutation. In addition to the stator, rotor, and ESC, BLDC motors can include position sensors such as optical encoders or Hall effect sensors to monitor the rotor position and perform the commutation more effectively. These sensors can significantly impact motor efficiency, reliability, and performance [7]; and as a result, larger BLDC motors typically use such sensors.

The family of BLDC motors subdivides into two distinctive categories: axial flux and radial flux motors. Radial flux motors are more common, being studied and used in a larger number of applications. However, some research suggests that the axial flux design may yield a smaller, lighter, and more efficient motor [8,9]. Although promising, current research on axial flux motors limits their use in hand-size UAVs (i.e., in the range of 50 W). Furthermore, axial flux motors of this power range are not readily available commercially.

Among radial flux motors, there are two subcategories: inrunner and outrunner motors. The former has the stator surrounding the rotor while in the latter, the rotor surrounds the stator. The advantage of outrunner BLDC motors is that they have lower speeds and higher torque making them useful for direct-drive applications as in [2, 5, 10, 11]. Here, the rotor shaft is directly fixed to a propeller without any gearing thereby reducing the weight and complexity of the vehicle, eliminating transmission losses, and reducing costs.

The design of a UAV entails the proper selection of a motor and propeller combination. In order to perform this selection, it is important to quantify the speed-voltage and torque-current characteristics of the motor as well as the

Received 29 September 2016; Revised 30 May 2017; Accepted 30 May 2017; Published 1 August 2017. This paper was accepted for publication in the Special issue on Aerial Robotics: Success Stories of Today and Hopes of Tomorrow. Guest Editors: Farrokh Janabi Sharifi, Youmin Zhang, Hossein Bonyan Khamseh and Howard Li.
Email Address: *eric.lanteigne@uottawa.ca
*Corresponding author.

speed-torque-thrust characteristics of propellers. Since motors and propellers have narrow bands of high efficiency operating conditions, a proper selection identifies a propeller which will produce enough thrust to maintain a steady flying altitude while turning at a speed which is optimal for the motor-propeller combination's performance.

BLDC motor manufacturers rarely include test data identifying the motors' operating characteristics. Instead, general motor characteristics are given such as the speed constant, the winding resistance, and the current at no-load. Similarly, propeller manufacturers for use in small air-crafts provide very little information about the propeller's performance or geometry. The only data consistently provided are the propeller's diameter and pitch.

Although accurate models are important when developing UAV control systems, it can be useful to quickly approximate motor and propeller performance without the hassle of measuring and testing the products in a laboratory setting. Therefore, this paper aims to validate simple models with the purpose of canvassing the market for an appropriate BLDC motor and propeller combination. The paper expands on the results presented in [12] by providing theoretical and experimental wind tunnel data on motor and propeller combinations at typical UAV operating speeds.

2. Modeling

2.1. *Modeling BLDC motors*

Permanent magnet motors are characterized by a linear correlation between the angular speed and the electromotive force (EMF), as well as between the torque and the current [13]. Typical theoretical BLDC motor characteristics are shown Fig. 1. This plot illustrates that the torque and the current are proportional, and that both linearly decrease with increasing angular speed given a constant driving voltage. In addition, a lower driving voltage, as defined by the voltage supply percentage β, yields lower speeds and torques.

The relation between torque and speed is explained by a motor circuit analysis. Consider the simplified motor (M), source (S), and electronic speed controller (ESC) circuit shown in Fig. 2. The supply voltage, V_s, the back EMF produced by rotation, E_b, the line-peak current passing through the windings, i, and the motor winding resistance, R_m, are related by Kirchoff's voltage law: $V_s = E_b + iR_m$. It follows that for a fixed supply voltage, the back EMF and current are inversely proportional: $E_b \propto \frac{1}{i}$. Given that the torque is proportional only to the current, a fixed load will draw a fixed amount of current and the remaining difference will be back EMF ($V_s - iR_m = E_b$). As the load increases,

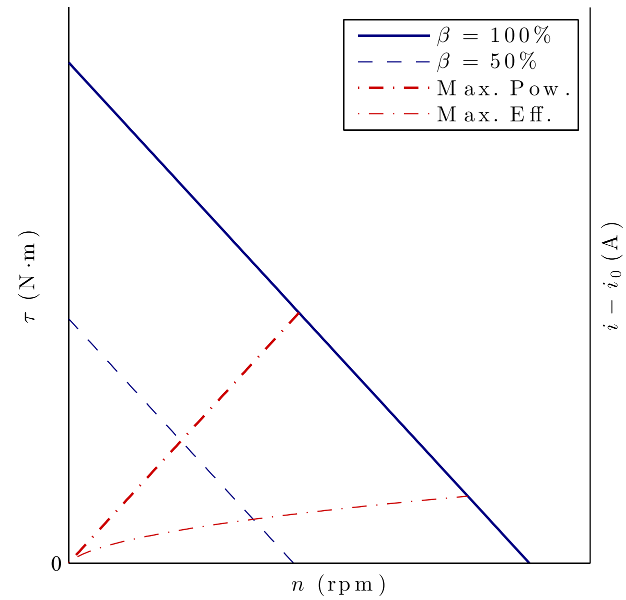

Fig. 1. Theoretical speed-torque-current characteristics of a BLDC motor at a constant driving voltage.

more current is drawn, the remaining E_b is smaller, and the motor decelerates.

The fact that motor speed is dependent on load makes the speed difficult to control. Electronic speed controllers (ESCs) are used to overcome this dependency and allow the control of speed independently of torque through the use of pulse width modulation (PWM). PWM is the rapid connection/disconnection of the power supply to mimic the effect of a lower supply voltage and shift the speed-torque curve downwards, or to the left. The effect of the ESC is shown by the dashed line $\beta = 50\%$ in Fig. 1. In this example, the ESC is mimicking the effect of a supply voltage 50% smaller than that actually being used.

The linear relations between the speed and EMF as well as between the torque and current are provided in Eqs. (1) and (2). Their proportionality constants are respectively called the motor's speed constant, K_v (rpm/V), and torque constant, K_t (N · m/A). The relationships are:

$$n = K_v E_b = K_v(v - iR_m), \tag{1}$$

$$\tau = K_t(i - i_0), \tag{2}$$

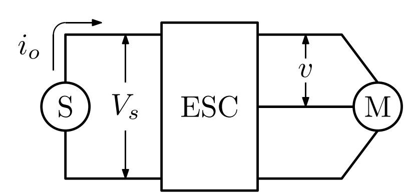

Fig. 2. Simplified circuit diagram of a BLDC motor with electronic speed control.

where n is the motor's shaft speed (rpm), τ is its output torque ($\mathrm{N} \cdot \mathrm{m}$), R_m is its winding resistance (Ω), i is its line-peak current (A), and i_0 represents the motor's line-peak current at no-load (A). The current at no-load is subtracted in Eq. (2) because this minimum amount of current is required to overcome the motor's intrinsic mechanical resistance.

The voltage, v, in Eq. (1) would usually be the source voltage which supplies the motor. However, this would mean that the motor model only predicts performance when the ESC is running at a duty cycle of 100% (i.e., when there is effectively no PWM). Instead, it is more valuable to define v as the apparent voltage seen by the motor as a result of the ESC's PWM. This way, the apparent voltage can be varied so the motor model can cover the full spectrum of possible speed-torque outputs. In order to define v, the ESC's effects need to be modeled as well. Let

$$v = f(V_s, \epsilon), \tag{3}$$

where f is a function of the source voltage, V_s, and the ESC's signal, ϵ, in μs. The function f must be defined such that the motor's output speed is equal if the motor is run with (a) a source V_s and an arbitrary ESC signal of ϵ or (b) a source of $v < V_s$ and an ESC signal of $\epsilon = 2000\,\mu$s (the ESC signal for 100% duty cycle). An experimental method for identifying f is presented in Sec. 4.

The motor constants K_v and K_t in Eqs. (1) and (2) may also be related. In the case of an ideal brushed DC motor (in which saturation and losses are neglected), the motor speed and torque constants are related through energy conservation by $P = E_b i = \tau\omega$ such that:

$$K_t = \frac{60}{2\pi K_v}. \tag{4}$$

Hendershot and Miller stress the importance of how motor constants are defined, particularly K_t as it depends on the phase wave shape and phase shift, and is temperature dependent [13]. The relation in Eq. (4) holds true for ideal brushed DC motor as well as ideal BLDC motors with squarewave drives in which Eq. (2) relates torque to the line-peak current. However, the relation must be multiplied by the factor $\sqrt{3/2}$ if Eq. (2) is based on the RMS current. Similar conversions are provided in [13] for motors with sinewave drives drives.

Equations (1)–(4) fully define the motor's operating condition (τ and n) as a function of the ESC's signal and the drawn current using only motor data provided by the manufacturer (K_v, i_0, R_m, and V_s). These equations can also be used to identify the driving currents for two operating conditions of particular interest: the points of maximum efficiency and of maximum power. The efficiency can be expressed as the ratio of useful mechanical power output to the electrical power input. Substituting τ and n by the expressions in Eqs. (1) and (2), the efficiency is given by

$$\eta = \frac{P_M}{P_E} = \frac{\tau\left(\frac{2\pi n}{60}\right)}{vi} = \frac{(v - iR_m)(i - i_0)}{vi}. \tag{5}$$

Then, taking the derivative of Eq. (5) with respect to current yields:

$$\frac{d\eta}{di} = \frac{i_0 v - i^2 R_m}{i^2 v} \tag{6}$$

and setting Eq. (6) to zero yields i_e, the driving current at maximum efficiency:

$$i_e = \sqrt{\frac{v i_0}{R_m}}. \tag{7}$$

A similar expression can be found for the driving current at peak power by starting with the equation for mechanical power and taking the derivative with respect to driving current.

$$P_M = \tau\left(\frac{2\pi n}{60}\right) = (v - iR_m)(i - i_0), \tag{8}$$

$$\frac{dP_M}{di} = v - 2iR_m + i_0 R_m. \tag{9}$$

Setting the result to zero then yields i_p, the driving current at peak power:

$$i_p = \frac{v + R_m i_0}{2R_m}. \tag{10}$$

The points of maximum efficiency and peak power are functions of the motor's characteristics. They may be drawn on the speed-torque plot to identify optimal operating conditions as shown by the dotted lines in Fig. 1. This information alone would be useful if the propeller torque and speed were known and the objective was to source an appropriate BLDC motor. However, manufacturers currently do not provide this data.

2.2. *Modeling propellers*

An accurate propeller model should account for the geometric properties such as the blade diameter, blade angle (i.e., pitch), chord length, shape of the airfoil, as well as the way in which each of those parameters varies with respect to radial distance. In addition to the geometric properties, one has to account for the airflow into the propeller, how the flow is modified as it exits the propeller, and how these flows may change as the aircraft travels in any direction.

Since a comprehensive model is complex, it is common to characterize a propeller's performance by non-dimensional coefficients for the thrust, torque, power, efficiency, etc. These coefficients are determined experimentally through either static bench tests or dynamic tests in a wind tunnel.

In this paper, only one nondimensional coefficient is presented: the thrust coefficient. As shown in [14], that nondimensional coefficient can be used to obtain values for T, the dynamic thrust (N), in the following way

$$T = C_T \rho \pi d^4 \omega^2, \tag{11}$$

where C_T is the nondimensional thrust coefficient, ρ is the density of the fluid (kg/m^3), d is the blade diameter (m), and ω is the propeller's angular velocity (rad/s).

Some researchers have attempted to determine C_T analytically but this requires detailed knowledge of the propellers geometry. Instead, an alternative model for the dynamic thrust of propellers is introduced. The relation, proposed by Staples [15], was developed from simple momentum theory and then fit to experimental data. It is of the form:

$$\begin{aligned} T = \rho\pi \frac{(0.0254 \cdot d)^2}{4} \left(\frac{n}{60} \cdot 0.0254 \cdot p\right) \\ \times \left(\left(\frac{n}{60} \cdot 0.0254 \cdot p\right) - V_0\right) \left(\frac{d}{K_1 \cdot p}\right)^{K_2}, \end{aligned} \tag{12}$$

where p is the propeller's pitch (in), n is its speed (rpm), and V_0 is the wind speed (m/s). The constants $K_1 = 3.29546$ and $K_2 = 1.5$ were empirically determined to fit the model with experimental data. Rearranging Eq. (12) to resemble Eq. (11), a generalized, empirically correlated, thrust coefficient can be obtained as a function of propeller diameter and pitch.

$$\begin{aligned} C_T = \left(\frac{60}{2\pi}\right)^2 \frac{0.0254^4}{4 \cdot 60^2} \\ \times \left(1 - \frac{V_0 \cdot 60}{n \cdot 0.0254 \cdot p}\right) K_1^{-K_2} \left(\frac{d}{p}\right)^{K_2 - 2}. \end{aligned} \tag{13}$$

In Eqs. (12) and (13), setting the wind speed to zero yields equations for the static thrust and static thrust coefficient as presented in [12]. These equations are respectively:

$$T = \rho\pi \frac{(0.0254 \cdot d)^2}{4} \left(\frac{n}{60} \cdot 0.0254 \cdot p\right)^2 \left(\frac{d}{K_1 \cdot p}\right)^{K_2}, \tag{14}$$

$$C_T = \left(\frac{60}{2\pi}\right)^2 \frac{0.0254^4}{4 \cdot 60^2} K_1^{-K_2} \left(\frac{d}{p}\right)^{K_2 - 2}. \tag{15}$$

3. Methodology

The models are validated by comparing theoretical predictions to experimental tests conducted on different motor and propeller combinations. In this paper, three of the 16 statically tested propellers in [12] are tested dynamically in a wind tunnel. The tests were conducted using the E-Flite Park480 motor with three APC propellers 9 inches in diameter with pitches of each 3.8, 6, and 7.5 inches.

3.1. *Theoretical predictions*

Theoretical motor predictions were made with the characteristics published by the manufacturer. This was based on the findings from [12] which showed that the published values for R_m agreed very well with experimentally gathered data while the values for i_0 have little impact on the model. The results from [12] showed a disagreement of over 15% in regards to K_v but it is suspected that the methods used to estimate K_v in that instance may not have been accurate.

The propeller's theoretical behaviors were also modeled using only the propeller's diameter and pitch as provided by the manufacturer.

3.2. *Experimental tests*

Experimental data were gathered using the RC Benchmark motor test stand used for the static and wind tunnel testing of motor-propeller combinations. The wind tunnel test setup is shown in Fig. 3. A 3D printed standoff (in blue) and counter weight (in red) were added to the test stand to operate the motor in the forward direction, opposite to the manufacturer's recommendations. This modification was made to fix the test stand downwind from the propeller. The power source voltage and current, motor mechanical speed (via the measurement of motor electrical speed), motor-propeller thrust, and torque were then measured at four different wind speeds.

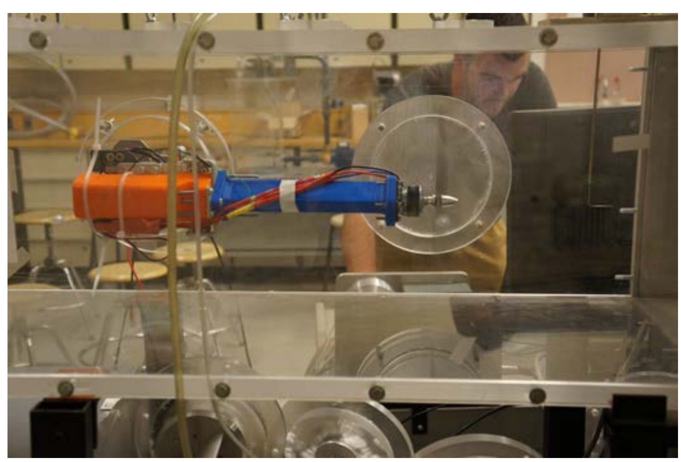

Fig. 3. Testing of motor-propeller in a wind tunnel.

4. Results

4.1. *Motor model & experimental results*

Figure 4 traces the theoretical BLDC model over the experimental results (shown in grey). The downward slopes represent the BLDC's theoretical speed-torque relationship at the apparent voltage levels of $v = 0.75\,V_s$ and $v = 1.00\,V_s$. These results are very similar to results gathered in [12].

In order to compare these predictions to the test data, the ESC transform $f(V_s, \epsilon)$ must be defined. The following test method was implemented to determine f: the motor is run statically outside the wind tunnel without a propeller. The use of a propeller would skew the results since the motor's speed would be dependent on the propeller's torque (which is in turn proportional to motor speed) in addition to the voltage and ESC signal. The test's objective is to find the driving voltage $v = v_x$ which, if run with $\epsilon = 2000\,\mu$s, will yield the same output speed as the motor running with $v = V_s$ and $\epsilon = \epsilon_x$. Take, for example, $\epsilon = 1500\,\mu$s. First, the motor is run with $v = V_s$ and $\epsilon = 1500\,\mu$s and the output speed is noted. Next, the motor is run with $v = V_s$ and $\epsilon = 2000\,\mu$s and the voltage is gradually reduced until at $v = 0.95\,V_s$ the same output speed is achieved.

The results are shown in Table 1. Unfortunately, minimal useful data could be obtained since the motor was unable to run steadily at low values of ϵ and saturated at high values of ϵ. As a result, the range for which n is linearly proportional to ϵ is limited. Another issue was that the motor was unable to run if the source voltage is lower than roughly 10 V. This further complicated the identification of f since there were very few points where a driving voltage v_x was found such that the motor speed when running with v_x and $\epsilon = 2000\,\mu$s was the same as when running with V_s and ϵ_x. Nevertheless, those few points were plotted with ϵ the independent variable and v the dependent to determine the first-order best fit line given by

$$v = 0.00348\epsilon + 5.64. \tag{16}$$

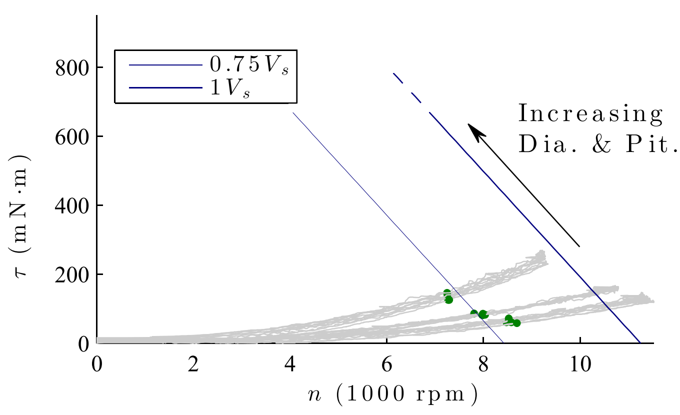

Fig. 4. Theoretical and experimental E-flite Park 480 motor performance.

Table 1. Experimentally determining the ESC's transform.

Step 1			Step 2		
v (%V_s)	ϵ (μs)	n (rpm)	v (%V_s)	ϵ (μs)	n (rpm)
100	2000	11 750	100	2000	11 750
100	1800	11 750	100	2000	11 750
100	1600	11 740	100	2000	11 740
100	1500	11 450	97.5	2000	11 450
100	1400	11 280	96	2000	11 280
100	1300	10 980	93.5	2000	10 980
100	1200	10 140	86.5	2000	10 140
100	1100	7 720	83	2000	9 200

Using this equation, an ESC signal of $\epsilon = 1410\,\mu$s yields an apparent voltage of 95%. Figure 4 shows the test data points, where $\epsilon = 1450\,\mu$s. These points are far below the theoretical predictions for an apparent driving voltage of $v = 0.95\,V_s$; in fact, they lie closer to the theoretical predictions for $v = 0.75\,V_s$. A closer look at Fig. 4 further discredits this definition of f since the trend line that would connect all the points would have a slope drastically shallower than that of the theoretical models.

One possibility, alluded to in [12], is that modeling the ESC is made difficult by the fact that the load is proportional the speed (as the propeller turns faster, it creates more thrust and more torque). As a result, an ESC transform identified with the proposed test method will accurately estimate the apparent voltage for use in Eq. (1) for only the scenario tested. In other words, to estimate the speed of a motor run with a 9×6 propeller, the ESC transform will need to be developed by performing the tests with that same 9×6 propeller. This is not an acceptable solution given that the objective is to quickly and simply estimate motor and propeller performance without the need for laboratory testing.

4.2. *Propeller model and experimental results*

The experimental results for three propellers are shown in Figs. 5–7 alongside the theoretical models for wind speeds from 0 m/s to 11 m/s. From these results, it is apparent that:

- At higher pitches, wind speed has less of an effect (the data is grouped closer together).
- At higher motor speeds, wind speed has less of an effect (the data converges as n increases).

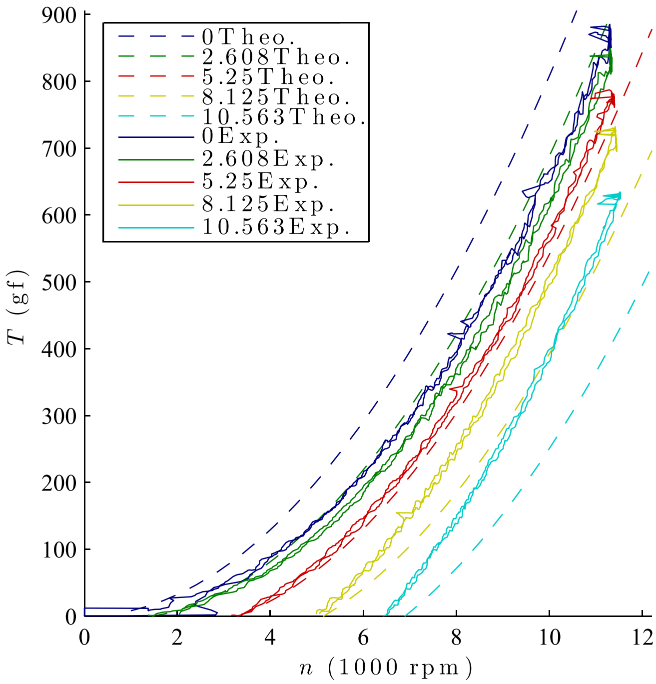

Fig. 5. Theoretical (dashed) and experimental (solid) 9×3.8 propeller performance at various wind speeds.

- For the 9×3.8 propeller, theoretical and experimental data agree very well at a wind speed of about 5.4 m/s. The model overestimates thrust for lower wind speeds and underestimates thrust for higher wind speeds.

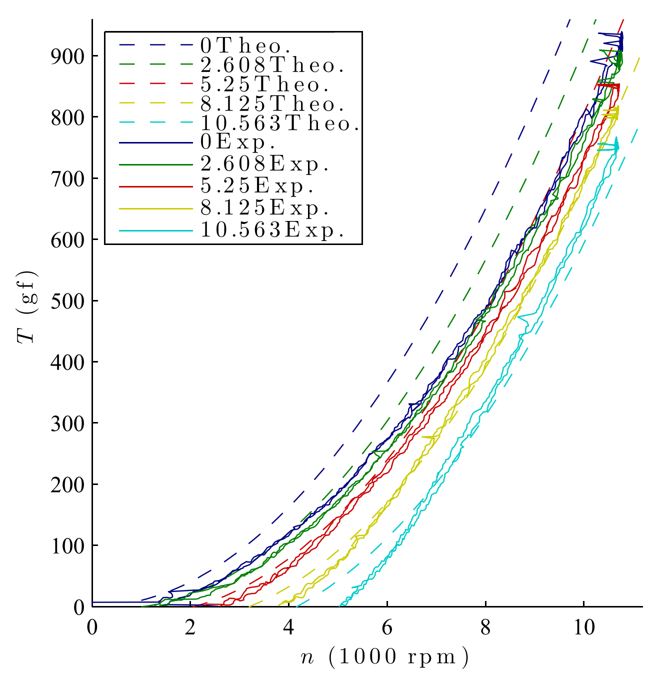

Fig. 6. Theoretical (dashed) and experimental (solid) 9×6 propeller performance at various wind speeds.

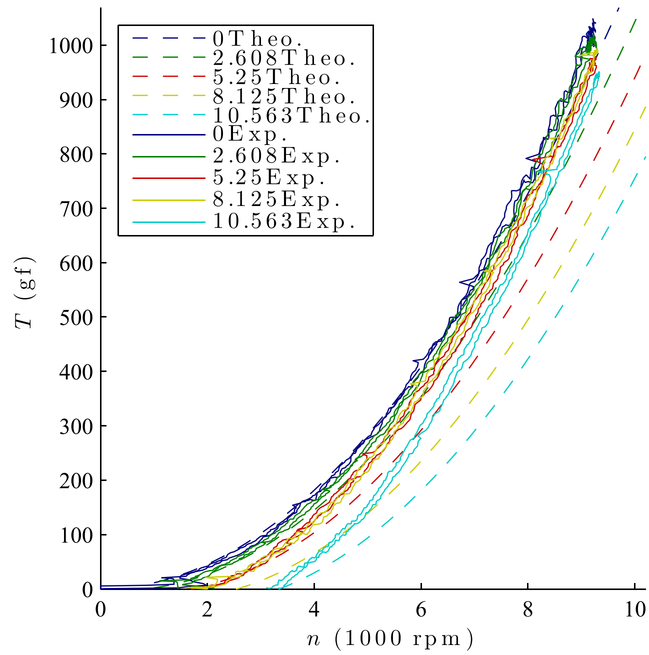

Fig. 7. Theoretical (dashed) and experimental (solid) 9×7.5 propeller performance at various wind speeds.

- For the 9×6 propeller, theoretical and experimental data agree very well at a wind speeds higher than 8 m/s. The model overestimates thrust for lower wind speeds.

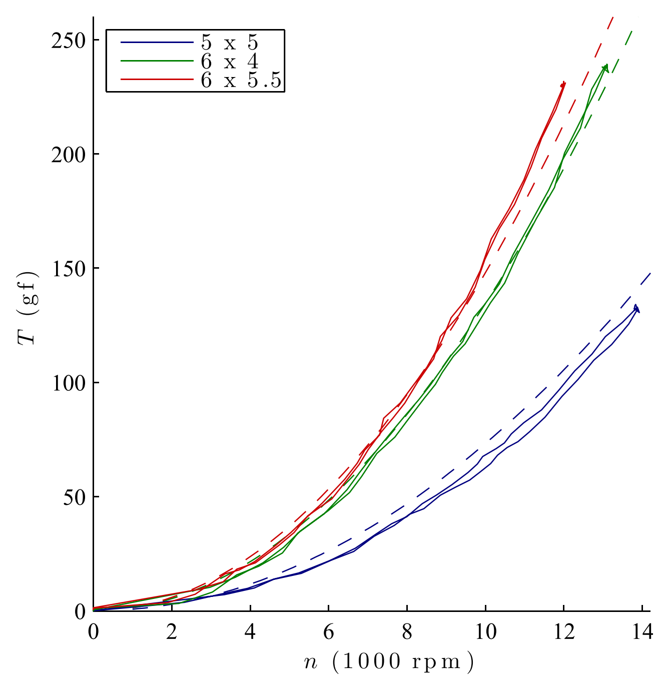

Fig. 8. Modified theoretical (dashed) and experimental (solid) 5″ and 6″ static propeller performance.

The model's constants K_1 and K_2 can be altered to yield more accurate results. For example, in Fig. 8, the constants $K_1 = 1.7$ and $K_2 = 3.8$ were determined by trial and error to show how K_1 and K_2 can affect the model. A more rigorous approach would be to write a program which would iteratively try different values and calculate the average error on all propellers in order to select the constants which minimize the error.

It is easy to adjust C_T's sensitivity to different variables (e.g., V_0, n, p, etc.) by modifying the constants K_1 and K_2 or by introducing new constants. However, it is quintessential to keep sample size in mind. As in [12], the modified constants may be better suited to this particular set of data while Staples' coefficients may be more generalized. A broader study could integrate data gathered and published by other sources, such as [16], to identify generalized constants for use in Eq. (13), or specialized constants tailored to a specific range of diameters or pitches.

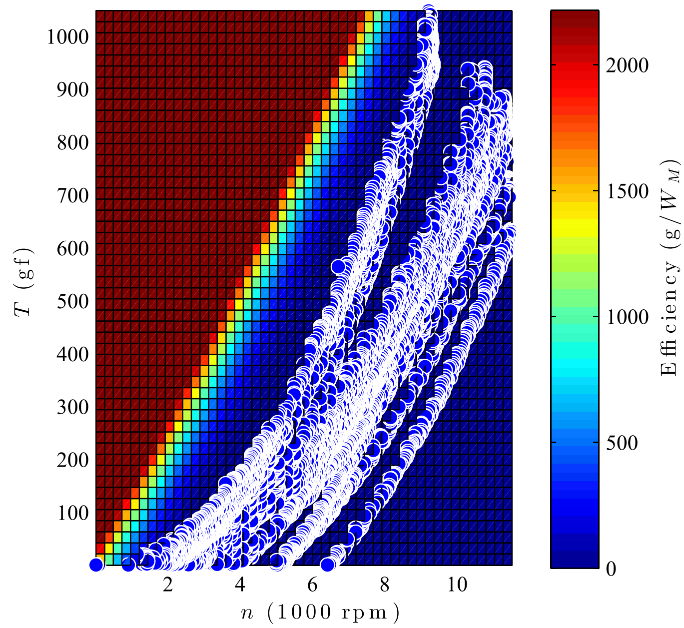

Fig. 10. Propeller efficiency map.

4.3. *Efficiency mapping*

Having measured the thrust, torque, speed, voltage, and current in various tests, it is possible to calculate the efficiency of the hardware. In particular, it is possible to calculate the efficiency of the motor independently of the efficiency of the propellers as well as calculate the efficiency of the motor and propeller combination.

The efficiency maps for the wind tunnel test are shown in Figs. 9–11. These maps are interesting because they reflect the data gathered from a larger number of tests. The efficiency maps are created by fifth-order polynomial interpolation over the data points collected in the motor-propeller tests. The electric power is calculated as the product of instantaneous voltage and current while the mechanical power is the product of instantaneous torque and angular speed. The motor, propeller, and combined

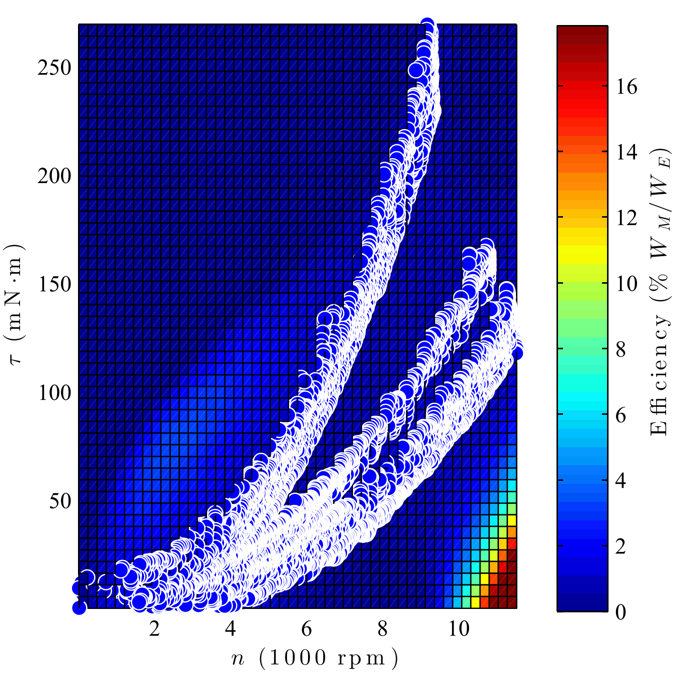

Fig. 9. E-flite Park 480 motor efficiency map.

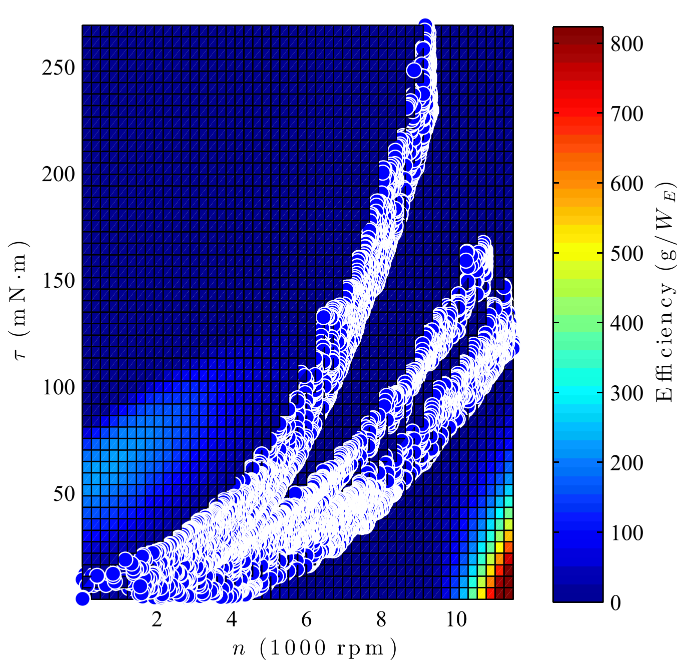

Fig. 11. E-flite Park 480 motor-propeller efficiency map.

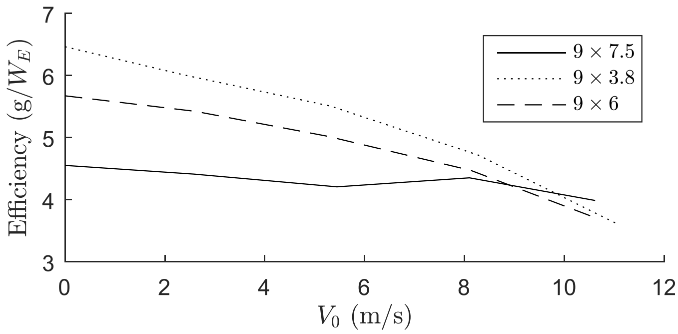

Fig. 12. Experimental E-flite Park 480 motor-propeller efficiency at $\epsilon = 1400\,\mu$s.

efficiency maps respectively show interpolated surfaces for the ratio of mechanical to electrical power ($\%W_M/W_E$), the ratio of thrust to mechanical power (gf/W_M), and the ratio of thrust to electrical power (gf/W_E). The effects of the wind speed on the motor-propeller efficiency are shown in Figs. 12–14. As predicted from Eq. (12), the combined efficiency decreases with increased with increasing wind speed. However, it is interesting to note that for that the magnitude of the trends are not consistent across all propellers. Although the 9 × 6 propeller and motor combination produced a lower thrust per watt than the two other

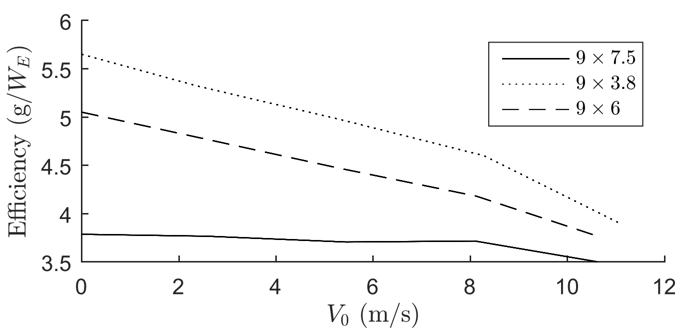

Fig. 13. Experimental E-flite Park 480 motor-propeller efficiency at $\epsilon = 1500\,\mu$s.

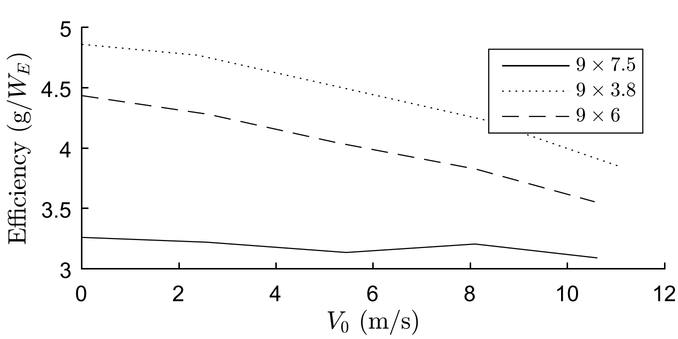

Fig. 14. Experimental E-flite Park 480 motor-propeller efficiency at $\epsilon = 1600\,\mu$s.

propellers, it's efficiency was approximately constant over a wide range of wind speeds.

5. Discussion

The proposed ESC model was shown to incorrectly represent its effects on motor performance. The model was defined as a function $f(V_s, \epsilon)$ which would yield an apparent driving voltage v for use in the equation $n = K_v(v - iR_m)$. However, this definition is inherently incorrect because the parameters V_s and ϵ do not fully define the motor's state nor determine the motor torque. This means that rather than specifying a point (n, τ) on the motor's speed-torque plot, the parameters V_s and ϵ correspond to a slope parallel and to the left of the motor's maximum n-τ relation. This same obstacle that was encountered in [12] and is the reason that the experimental results seemed to indicate that the motor model was inaccurate.

Second, since the ESC model does not provide a suitable means of identifying specific operating points (n, τ), the motor model's accuracy is undetermined. However, there is evidence to suggest that the model has faults. For example, when the motor and 9 × 3.8 propeller are run at full speed, the experimentally measured operating condition (n, τ) surpasses the model's theoretical limits. Similar results were found in [12] and the conclusion had been that the motor data provided by manufacturer (particularly K_v) was inaccurate. In order to validate the motor model, tests should be run on a motor with a mechanical brake applying the external load. This way, all the parameters which determine the motor's operating condition (i.e., $i \propto \tau$, V_s, and ϵ) can each be independently be varied or held fixed.

Lastly, this paper demonstrated that Staples' relation is fairly accurate in estimating the thrust for dynamically tested propellers. The equations constitute an interesting alternative to conventional propeller thrust estimations given their simplicity. As mentioned above, it would be interesting to apply these equations to a larger number of propellers in an effort to determine more generalized constants or constants better suited to niches of propellers with particular diameters and pitches. Furthermore, it would be interesting to investigate if a relation could be developed for the propeller's torque coefficient. If both the

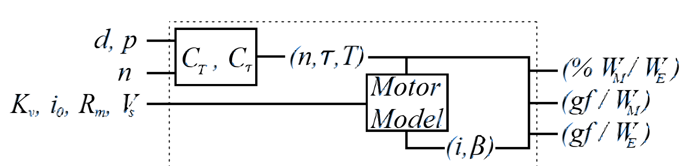

Fig. 15. Inputs and outputs to the coupled thrust-torque models.

thrust and torque could be estimated as a function of speed, then it would make it possible to couple the theoretical motor and propeller models by using the propeller model's outputs as inputs to the motor model as shown in Fig. 15.

6. Conclusion

This paper aimed to validate simple motor and propeller models with the purpose of selecting an appropriate motor-propeller combination across a range of wind speeds. It was possible to independently validate the propeller models by decoupling them and studying the results separately. These results could facilitate the selection of hardware if one or both of the operating conditions are predetermined. Maximizing efficiency is then a question of choosing a motor and/or propeller such that the efficiency is maximized for the operating speed and thrust.

Acknowledgment

This work was supported by the NSERC Discovery Grant RGPIN-2014-04501.

References

[1] S. Recoskie, A. Fahim, W. Gueaieb and E. Lanteigne, Experimental testing of a hybrid power plant for a dirigible UAV, *J. Intell. Robot. Syst.* **69**(1–4) (2013) 69–81.

[2] P. Pounds, R. Mahony and P. Corke, Modelling and control of a large quadrotor robot, *Control Eng. Pract.* **18**(7) (2010) 691–699.

[3] S. Diressens and P. Pounds, Towards a more efficient quadrotor configuration, *Int. Conf. Intelligent Robots and Systems* (November 2013), Tokyo, Japan, pp. 691–699.

[4] P. Pounds, R. Mahony, J. Gresham, P. Corke and J. M. Roberts, Towards dynamically-favourable quad-rotor aerial robots, *Australasian Conference on Robotics & Automation* (Canberra, Australia, 2004), pp. 1386–1392.

[5] P. Lindahl, E. Moog and S. R. Shaw, Simulation, design, and validation of an UAV SOCF propulsion system, *IEEE Trans. Aerosp. Electron. Syst.* **48**(3) (2012) 2582–2593.

[6] W. Khan and M. Nahon, Toward an accurate physics-based UAV thruster model, *IEEE/ASME Trans. Mechatronics* **18**(4) (2013) 1269–1279.

[7] Honeywell, *How to Select Hall-Effect Sensors for Brushless DC Motors*, (Honeywell International Inc., 2015).

[8] K. Sitapati and R. Krishnan, Performance comparisons of radial and axial field, permanent-magnet, brushless machines, *IEEE Trans. Ind. Appl.* **37** (2001) 1219–1226.

[9] A. Cavagnino, M. Lazzari, F. Profumo and A. Tenconi, A comparison between the axial flux and the radial flux structures for PM synchronous motors, *IEEE Trans. Ind. Appl.* **38** (2002) 1517–1524.

[10] S. Recoskie, Autonomous hybrid powered long range airship for surveillance and guidance, PhD thesis, University of Ottawa (2014).

[11] A. Imam and R. Bicker, Design and construction of a small-scale rotorcraft UAV system, *Int. J. Eng. Sci. Innov. Technol.* **2** (2014) 96–109.

[12] D. Muzar and E. Lanteigne, Experimental characterization of brushless dc motors and propellers for small aerial vehicles, *CSME International Congress*, Canadian Society for Mechanical Engineering International Congress (Kelowna, Canada, 2016), pp. 1–6.

[13] J. R. Hendershot and T. J. E. Miller, *Design of Brushless Permanent-Magnet Machines* (Motor Design Books, 2010).

[14] J. Seddon, *Basic Helicopter Aerodynamics* (American Institute of Aeronautics and Astronautics, 1990).

[15] G. Staples, Propeller static and dynamic thrust calculation (2013). www.electricrcaircraftguy.com/2013/09/propeller-static-dynamic-thrust-equation.html. Accessed on 01/09/2016.

[16] J. B. Brandt, R. W. Deters, G. K. Ananda and M. S. Selig, UIUC propeller database, technical report, University of Illinois at Urban-Champaign (2015).

Eric Lanteigne received his B.Sc.A. in 2003 and M.Sc.A. in 2006, both in Mechanical Engineering and from the University of Ottawa. In 2011 he received his Ph.D. in Mechanical Engineering from the Royal Military College of Canada. He then joined the Department of Mechanical Engineering at the University of Ottawa in August 2011 as assistant professor. Professor Lanteigne has worked on a number of design projects including the development of miniature manipulators, track-mounted mobile robots for the agricultural industry, mechanisms for drying pipes for the trench-less rehabilitation of municipal water mains, stair-climbing robots, and UAVs. His research area is unmanned aerial vehicle and mobile robot design with a focus on small airships and blimps.